International Journal of Solids and Structures 80 (2016) 381–392

Contents lists available at ScienceDirect

International Journal of Solids and Structures

journal homepage: www.elsevier.com/locate/ijsolstr

Influence of second-phase inclusions on the electro-deformation of ferroelectric ceramics

Cristian J. Bottero [a,b], Martín I. Idiart [a,b,*]

[a] Departamento de Aeronáutica, Facultad de Ingeniería, Universidad Nacional de La Plata, Avda. 1 esq. 47 S/N, La Plata B1900TAG, Argentina
[b] Consejo Nacional de Investigaciones Científicas y Técnicas (CONICET), CCT La Plata, Calle 8 N° 1467, La Plata B1904CMC, Argentina

ARTICLE INFO

Article history:
Received 7 March 2015
Revised 19 August 2015
Available online 26 October 2015

Keywords:
Composites
Porosity
Ferroelectricity
Homogenization
Hysteresis

ABSTRACT

Theoretical estimates are given for the overall dissipative response of ferroelectric ceramics with second-phase inclusions, under arbitrary electromechanical loading histories. The ferroelectric behavior of the constituent phases is described via a stored energy density and a dissipation potential in accordance with the theory of generalized standard materials. An implicit time-discretization scheme is used to generate a variational representation of the overall response in terms of a single incremental potential. Estimates are then generated by constructing sequentially laminated microgeometries of particulate type whose overall incremental potential can be computed exactly. Because they are realizable, by construction, these estimates are guaranteed to conform with any material constraints, to satisfy all pertinent bounds, and to exhibit the required convexity properties with no duality gap. By way of example, the theory is used to study the influence of metallic particles and of microcavities on the electro-deformability of a lead zirconate titanate. In particular, the role of remanent polarization fluctuations on the piezoelectric properties is assessed.

1. Introduction

The search for electro-deformable materials with specific combinations of properties not found in monolithic ferroceramics has motivated the development of an increasing variety of two-phase ferroelectric composites. A natural option consists in dispersing in a polycrystalline ferroelectric ceramic second-phase inclusions such as metallic particles (e.g., Duan et al., 2000; Ning et al., 2012; Zhang et al., 2010) or microcavities (e.g., Piazza et al., 2010). In practice, these composite materials are first synthesized by a suitable fabrication process, then permanently polarized by application of a strong electric field, and finally employed within their piezoelectric regime. Now, the influence of a second phase on the final piezoelectric properties of the composite system is not evident a priori in view of the intrincated role of material heterogeneity in the poling process. The purpose of this work is to estimate theoretically such influence in terms of the constitutive properties of the phases and the microstructural characteristics of the composite. A wide range of micromechanical models have already been proposed for that purpose —see, for instance, the monograph of Topolov and Bowen (2009)—, but all proposals invariably treat the ferroceramic matrix of a poled composite as a stress-free phase with uniform piezoelectric properties. Due to material heterogeneity, however, strong spatial variations of the electric field can arise during the poling process which, in turn, can result in residual stresses and non-uniform piezoelectric coefficients within the permanently poled specimen (e.g., Idiart, 2014). To account for these features, the entire poling process must be simulated.

Given that ferroelectricity is largely hysteretic, the problem calls for a methodology to estimate the overall response of two-phase deformable dielectrics with complex particulate microstructures and with constituent phases that can simultaneously store and dissipate electro-mechanical energy. Estimates of this sort for *rigid* dielectrics have been recently derived by Idiart (2014). These estimates rely on the generalized-standard material model for ferroelectricity proposed by Bassiouny et al. (1988) —which identifies the irreversible electric polarization as an internal variable— and on the variational representation of Miehe and Rosato (2011) for the macroscopic response of heterogeneous ferroelectric solids in terms of an effective incremental potential. A special class of microgeometries is then identified such that it reproduces the essential geometrical features of the actual composite microstructure while at the same time allow the exact computation of this effective potential. The class consists of certain sequentially laminated microgeometries which have been successfully used already to model other types of particulate systems with nonlinear behavior such as viscoplastic composites and porous

* Corresponding author at: Departamento de Aeronáutica, Facultad de Ingeniería, Universidad Nacional de La Plata, Avda. 1 esq. 47 S/N, La Plata B1900TAG, Argentina. Tel.: +542214236679.

E-mail addresses: cristian.bottero@ing.unlp.edu.ar (C.J. Bottero), martin.idiart@ing.unlp.edu.ar, martin.idiart@gmail.com (M.I. Idiart).

http://dx.doi.org/10.1016/j.ijsolstr.2015.09.009
0020-7683/

media (e.g., Danas et al., 2008; deBotton and Hariton, 2002; Idiart, 2008), and non-ohmic composite conductors (Hariton and deBotton, 2003; Idiart and Ponte Castañeda, 2013). The predictions always conform with material constraints, satisfy all pertinent bounds, and exhibit the required convexity when applicable. This consistency is guaranteed by the fact that the estimates are realizable —i.e., exact for a given class of material systems— by construction. The present work provides a generalization of this approach to *deformable* dielectrics.

We begin in Section 2 by formulating the problem of a heterogeneous dielectric body undergoing small deformations. The overall response is defined for a general composite system in Section 3 and then given for sequentially laminated systems in Section 4. By way of example, specific results are reported in Section 5 for a lead zirconate titanate with either metallic particles or microcavities. We conclude the presentation by identifying a potential issue with a class of constitutive models commonly used for monolithic polycrystalline ferroceramics.

2. The composite material model

2.1. The material system and field equations

The material system under study is idealized here as a heterogeneous body occupying a domain Ω and made up of a continuous matrix containing a uniform dispersion of second-phase inclusions. The matrix phase will be identified with the index $r = 1$ while the inclusions will be collectively identified with the index $r = 2$. Each phase occupies a domain $\Omega^{(r)} \subset \Omega$ $(r = 1, 2)$ such that $\Omega = \Omega^{(1)} \cup \Omega^{(2)}$. The domains $\Omega^{(r)}$ are described by a set of characteristic functions $\chi^{(r)}(\mathbf{x})$, which take the value 1 if the position vector $\mathbf{x}$ is in $\Omega^{(r)}$ and 0 otherwise.

We restrict attention to isothermal processes produced by quasistatic electromechanical interactions. These interactions are exerted by a fixed electrostatic potential $\hat{\phi}$ applied via surface electrodes occupying a portion $\partial\Omega_v$ of the body boundary $\partial\Omega$ and by a surface displacement $\hat{\mathbf{u}}$ applied on a portion $\partial\Omega_u$ of the body boundary. For simplicity, we disregard the possible presence of free charges within the material. The governing field equations are then given by —see, for instance, Kamlah (2001)—

$$\nabla \cdot \mathbf{D} = 0 \quad \text{and} \quad \mathbf{E} = -\nabla\phi \quad \text{in } \mathbb{R}^3, \tag{1}$$

$$\nabla \cdot \boldsymbol{\sigma} = 0 \quad \text{and} \quad \boldsymbol{\varepsilon} = \nabla \otimes_s \mathbf{u} \quad \text{in } \Omega, \tag{2}$$

with

$$\mathbf{D} = \begin{cases} \epsilon_0 \mathbf{E} & \text{in } \mathbb{R}^3 \backslash \Omega \\ \epsilon_0 \mathbf{E} + \mathbf{P} & \text{in } \Omega \end{cases} \tag{3}$$

and boundary conditions

$$\phi = \hat{\phi} \quad \text{on } \partial\Omega_v \quad \text{and} \quad [\mathbf{D} \cdot \mathbf{n}] = 0 \quad \text{on } \partial\Omega \backslash \partial\Omega_v, \tag{4}$$

$$\mathbf{u} = \hat{\mathbf{u}} \quad \text{on } \partial\Omega_u \quad \text{and} \quad [\boldsymbol{\sigma}\mathbf{n}] = \mathbf{0} \quad \text{on } \partial\Omega \backslash \partial\Omega_u. \tag{5}$$

In these expressions, ϕ and $\mathbf{u}$ are continuous fields representing the electrostatic potential and the displacement, **D, E, P**, $\boldsymbol{\sigma}$ and $\boldsymbol{\varepsilon}$ are, respectively, the electric displacement, the electric field intensity, the material polarization, and the stress and strain tensors, $[\cdot]$ denotes the jump across $\partial\Omega$, $\mathbf{n}$ is the outward normal vector to $\partial\Omega$, and ϵ_0 denotes the electric permittivity of vacuum. In turn, ∇ is the standard nabla operator and the symbol $\otimes_s$ represents the symmetric part of the tensor product. Along internal surfaces of discontinuity, the various fields must satisfy the jump conditions

$$[\phi] = 0, \qquad [\mathbf{D} \cdot \mathbf{n}] = 0, \qquad [\mathbf{u}] = 0, \qquad [\boldsymbol{\sigma}\mathbf{n}] = \mathbf{0}, \tag{6}$$

where $\mathbf{n}$ denotes the normal vector to the discontinuity surface. In addition, the electrostatic potential must vanish at infinity, i.e., $\phi \to 0$ as $|\mathbf{x}| \to \infty$.

The above field equations must be supplemented with constitutive relations describing the electromechanical response of each phase. We adopt the thermodynamic approach of Bassiouny et al. (1988) wherein dissipative processes are characterized by an irreversible polarization p playing the role of an internal variable. This framework is general enough to characterize simple responses such as linear polarizability as well as complex responses such as rate-dependent ferroelectricity —see, for instance, Kamlah (2001), Miehe and Rosato (2011).

The total energy of the material system and its surroundings is thus written as

$$\mathfrak{E} = \int_\Omega \mathfrak{e}(\mathbf{x}, \boldsymbol{\varepsilon}, \mathbf{P}, \mathrm{p})\, \mathrm{d}V + \int_{\mathbb{R}^3} \frac{1}{2}\epsilon_0 \mathbf{E}^2\, \mathrm{d}V \tag{7}$$

where the first term corresponds to the energy stored in the composite material while the second term is the electrostatic energy of the electric field. The energy density $\mathfrak{e}$ is taken to depend explicitly on position due to the heterogeneity of the body. In turn, the dissipation of the system is assumed to be of the form

$$\mathcal{D} = \int_\Omega \frac{\partial \varphi}{\partial \dot{\mathrm{p}}}(\mathbf{x}, \dot{\mathrm{p}}) \cdot \dot{\mathrm{p}}\, \mathrm{d}V, \tag{8}$$

where φ is a convex, positive function of the irreversible polarization rate $\dot{\mathrm{p}}$ such that $\varphi(\cdot, \mathbf{0}) = 0$, which is used to characterize the microscopic domain switching in the ferroelectric phase. The form (8) guarantees a positive dissipation.

Thermodynamic arguments then imply that the constitutive relations of the material are given by (see Bassiouny et al., 1988)

$$\mathbf{E} = \frac{\partial \mathfrak{e}}{\partial \mathbf{P}}(\mathbf{x}, \boldsymbol{\varepsilon}, \mathbf{P}, \mathrm{p}), \quad \boldsymbol{\sigma} = \frac{\partial \mathfrak{e}}{\partial \boldsymbol{\varepsilon}}(\mathbf{x}, \boldsymbol{\varepsilon}, \mathbf{P}, \mathrm{p})$$
$$\text{and} \quad \frac{\partial \mathfrak{e}}{\partial \mathrm{p}}(\mathbf{x}, \boldsymbol{\varepsilon}, \mathbf{P}, \mathrm{p}) + \frac{\partial \varphi}{\partial \dot{\mathrm{p}}}(\mathbf{x}, \dot{\mathrm{p}}) = \mathbf{0}, \tag{9}$$

where the first two expressions relate the electric field intensity and stress with the polarization and strain, and the last expression provides the evolution law for the irreversible polarization p. In the case of nonsmooth potentials, the derivatives in (9) should be understood in the sense of the subdifferential of convex analysis. These constitutive relations conform to the so-called generalized standard material model provided the energy $\mathfrak{e}(\mathbf{x}, \cdot, \cdot, \cdot)$ is convex (Germain et al., 1983). In that case, the polarization can be eliminated from the constitutive description in favor of the electric field intensity by defining the free energy density

$$\psi(\mathbf{x}, \boldsymbol{\sigma}, \mathbf{E}, \mathrm{p}) \doteq \sup_{\mathbf{P}, \boldsymbol{\varepsilon}} [\boldsymbol{\sigma} \cdot \boldsymbol{\varepsilon} + \mathbf{E} \cdot \mathbf{P} - \mathfrak{e}(\mathbf{x}, \boldsymbol{\varepsilon}, \mathbf{P}, \mathrm{p})] + \frac{1}{2}\epsilon_0 \mathbf{E}^2, \tag{10}$$

where the first term corresponds to a partial Legendre transformation of $\mathfrak{e}$ with respect to $\mathbf{P}$ and $\boldsymbol{\varepsilon}$. Note that the function ψ is thus convex in $\mathbf{E}$ and $\boldsymbol{\sigma}$ but concave in p. The constitutive relations (9) can then be written as

$$\mathbf{D} = \frac{\partial \psi}{\partial \mathbf{E}}(\mathbf{x}, \boldsymbol{\sigma}, \mathbf{E}, \mathrm{p}), \quad \boldsymbol{\varepsilon} = \frac{\partial \psi}{\partial \boldsymbol{\sigma}}(\mathbf{x}, \boldsymbol{\sigma}, \mathbf{E}, \mathrm{p})$$
$$\text{and} \quad \frac{\partial \psi}{\partial \mathrm{p}}(\mathbf{x}, \boldsymbol{\sigma}, \mathbf{E}, \mathrm{p}) - \frac{\partial \varphi}{\partial \dot{\mathrm{p}}}(\mathbf{x}, \dot{\mathrm{p}}) = 0. \tag{11}$$

Making use of the characteristic functions $\chi^{(r)}$, the potentials ψ and φ are finally expressed as

$$\psi(\mathbf{x}, \boldsymbol{\sigma}, \mathbf{E}, \mathrm{p}) = \sum_{r=1}^{2} \chi^{(r)}(\mathbf{x})\, \psi^{(r)}(\boldsymbol{\sigma}, \mathbf{E}, \mathrm{p}),$$
$$\varphi(\mathbf{x}, \dot{\mathrm{p}}) = \sum_{r=1}^{2} \chi^{(r)}(\mathbf{x})\, \varphi^{(r)}(\dot{\mathrm{p}}), \tag{12}$$

where $\psi^{(r)}$ and $\varphi^{(r)}$ denote, respectively, the free energy densities and dissipation potentials of each phase r.

The field equations and boundary conditions (1)–(6), together with the constitutive relations (11)–(12) and appropriate initial conditions, completely define the electromechanical response of the system under consideration.

2.2. Some material responses

Even though the approach considered in this work allows for general stored energy densities $\mathfrak{e}^{(r)}$ and dissipation potentals $\varphi^{(r)}$, it proves useful to record at this point some specific forms of common use.

(*i*) Many nonpolar solids can be characterized as ideal isotropic dielectrics with a non-dissipative linear response; in this case, the potentials are of the form

$$\mathfrak{e}^{(r)}(\boldsymbol{\varepsilon},\mathbf{P},\mathrm{p}) = \frac{1}{2}\boldsymbol{\varepsilon}\cdot\mathbb{C}^{(r)}\boldsymbol{\varepsilon} + \frac{1}{2}\mathbf{P}\cdot\boldsymbol{\kappa}^{(r)}\mathbf{P} \quad \text{and} \quad \varphi^{(r)}(\dot{\mathrm{p}}) = 0, \tag{13}$$

where $\boldsymbol{\kappa}^{(r)} = \kappa^{(r)}\mathbf{I}$ and $\mathbb{C}^{(r)} = \lambda^{(r)}\mathbf{I}\otimes\mathbf{I} + 2\mu^{(r)}\mathbb{I}$. Here, $\mathbf{I}$ and $\mathbb{I}$ are the second- and fourth-order identity tensors with major and minor symmetry, and $\kappa^{(r)}$, $\lambda^{(r)}$ and $\mu^{(r)}$ represent, respectively, the polarizability and Lamé constants of the solid; the free energy density is given by

$$\psi^{(r)}(\boldsymbol{\sigma},\mathbf{E},\mathrm{p}) = \frac{1}{2}\boldsymbol{\sigma}\cdot\mathbb{S}^{(r)}\boldsymbol{\sigma} + \frac{1}{2}\mathbf{E}\cdot\boldsymbol{\epsilon}^{(r)}\mathbf{E}, \tag{14}$$

where $\boldsymbol{\epsilon}^{(r)} = \epsilon_0\mathbf{I} + \boldsymbol{\kappa}^{(r)^{-1}} = \epsilon^{(r)}\mathbf{I}$ and $\mathbb{S}^{(r)} = (\mathbb{C}^{(r)})^{-1}$ represent, respectively, the permittivity and compliance tensors of the solid. The corresponding constitutive relations are given by

$$\boldsymbol{\varepsilon} = \mathbb{S}^{(r)}\boldsymbol{\sigma} \quad \text{and} \quad \mathbf{D} = \epsilon^{(r)}\mathbf{E}. \tag{15}$$

A perfect conductor where the electric field must vanish is characterized by the limiting case $\kappa^{(r)}\to 0$ ($\epsilon^{(r)}\to\infty$).

(*ii*) On the other hand, polycrystalline polar solids exhibiting isotropic ferroelectricity are commonly characterized by potentials of the form —see, for instance, Kamlah (2001), McMeeking and Landis (2002), Miehe and Rosato (2011)—

$$\mathfrak{e}^{(r)}(\boldsymbol{\varepsilon},\mathbf{P},\mathrm{p}) = \frac{1}{2}(\boldsymbol{\varepsilon}-\hat{\boldsymbol{\varepsilon}}^{(r)})\cdot\mathbb{C}^{(r)}(\boldsymbol{\varepsilon}-\hat{\boldsymbol{\varepsilon}}^{(r)}) + \frac{1}{2}(\mathbf{P}-\mathrm{p}) \cdot\boldsymbol{\kappa}^{(r)}(\mathbf{P}-\mathrm{p}) + (\boldsymbol{\varepsilon}-\hat{\boldsymbol{\varepsilon}}^{(r)})\cdot\mathbf{h}^{(r)}(\mathrm{p})(\mathbf{P}-\mathrm{p}) + \mathfrak{e}_{st}^{(r)}(\mathrm{p}) \tag{16}$$

and

$$\varphi^{(r)}(\dot{\mathrm{p}}) = e_c^{(r)}|\dot{\mathrm{p}}| + \frac{e_0^{(r)}\dot{p}_0^{(r)}}{1+m^{(r)}}\left(\frac{|\dot{\mathrm{p}}|}{\dot{p}_0^{(r)}}\right)^{1+m^{(r)}}, \tag{17}$$

where

$$\mathbb{C}^{(r)} = \lambda^{(r)}\mathbf{I}\otimes\mathbf{I} + 2\mu^{(r)}\mathbb{I}, \quad \boldsymbol{\kappa}^{(r)} = \kappa^{(r)}\mathbf{I}, \tag{18}$$

$$\mathfrak{e}_{st}^{(r)}(\mathrm{p}) = -h_0^{(r)}p_s^{(r)^2}\left[\ln\left(1-\frac{|\mathrm{p}|}{p_s^{(r)}}\right) + \frac{|\mathrm{p}|}{p_s^{(r)}}\right], \tag{19}$$

$$\hat{\boldsymbol{\varepsilon}}^{(r)}(\mathrm{p}) = \frac{3}{2}\varepsilon_s^{(r)}\left(\frac{|\mathrm{p}|}{p_s^{(r)}}\right)^2\frac{\mathrm{p}}{|\mathrm{p}|}\otimes_d\frac{\mathrm{p}}{|\mathrm{p}|}, \tag{20}$$

$$\mathbf{h}^{(r)}(\mathrm{p}) = \left(\alpha_0^{(r)}\frac{\mathrm{p}}{|\mathrm{p}|}\otimes\frac{\mathrm{p}}{|\mathrm{p}|}\otimes\frac{\mathrm{p}}{|\mathrm{p}|} + \alpha_\perp^{(r)}\mathbf{I}\otimes\frac{\mathrm{p}}{|\mathrm{p}|} + \alpha_=^{(r)}\frac{\mathrm{p}}{|\mathrm{p}|}\otimes_s\mathbf{I}\right) \times\frac{|\mathrm{p}|}{p_s^{(r)}}. \tag{21}$$

This model assumes that the polarization $\mathbf{P}$ and the strain $\boldsymbol{\varepsilon}$ are additive compositions of a reversible part $(\mathbf{P}-\mathrm{p})$ and $(\boldsymbol{\varepsilon}-\hat{\boldsymbol{\varepsilon}})$, and an irreversible part p and $\hat{\boldsymbol{\varepsilon}}$. The potentials $\mathfrak{e}_{st}^{(r)}$ and $\varphi^{(r)}$ represent the energy stored and dissipated via microdomain switching, and $\hat{\boldsymbol{\varepsilon}}$ is the remanent strain induced by this switching. In the energy function (16), $\mathbf{h}^{(r)}$ represents a piezoelectric coupling tensor and the $\alpha_i^{(r)}$ represent piezoelectric moduli. In the dissipation potential (17), $e_c^{(r)}$ is the coercive field strength of the solid —i.e., the electric field level above which domain switching is triggered—, $e_0^{(r)}$ and $\dot{p}_0^{(r)}$ are, respectively, a reference electric field and a polarization rate characterizing the rate-dependence of the switching process, and $m^{(r)}$ is a rate sensitivity exponent. In the stored energy density (19), in turn, $p_s^{(r)}$ is the saturation polarization and $h_0^{(r)}$ is a material parameter characterizing the electric hysteresis slope. In the remanent strain (20), $\varepsilon_s^{(r)}$ is the strain at saturated polarization, the symbol $\otimes_d$ denotes the deviatoric part of the tensor product, and the symbol $\otimes_s$ refers to symmetrization in the first two indices. The reader is referred to Miehe and Rosato (2011) for a detailed account of the various material parameters. It is noted that the connection (20) between the remanent strain and polarization simplifies the description for it allows the use of a single internal variable p. However, the resulting model is unable to capture ferroelasticity, that is, switching in response to stress, and introduces a non-convex dependence of $\mathfrak{e}^{(r)}$ on p which restricts the range of validity of the model to low mechanical stresses; this issue is discussed in Section 5.2. In any event, the corresponding free energy density within the convex range is given by

$$\psi^{(r)}(\boldsymbol{\sigma},\mathbf{E},\mathrm{p}) = \frac{1}{2}\boldsymbol{\sigma}\cdot\hat{\mathbb{S}}^{(r)}(\mathrm{p})\boldsymbol{\sigma} + \frac{1}{2}\mathbf{E}\cdot\hat{\boldsymbol{\epsilon}}^{(r)}(\mathrm{p})\mathbf{E} - \boldsymbol{\sigma}\cdot\hat{\mathbf{h}}^{(r)}(\mathrm{p})\mathbf{E} + \boldsymbol{\sigma}\cdot\hat{\boldsymbol{\varepsilon}}^{(r)}(\mathrm{p}) + \mathbf{E}\cdot\mathrm{p} - \mathfrak{e}_{st}^{(r)}(\mathrm{p}), \tag{22}$$

with

$$\hat{\mathbb{S}}^{(r)}(\mathrm{p}) = (\mathbb{C}^{(r)} - \mathbf{h}^{(r)}\boldsymbol{\kappa}^{(r)^{-1}}\mathbf{h}^{(r)T})^{-1}, \tag{23}$$

$$\hat{\boldsymbol{\kappa}}^{(r)} = \boldsymbol{\kappa}^{(r)} - \mathbf{h}^{(r)T}\mathbb{C}^{(r)^{-1}}\mathbf{h}^{(r)}, \tag{24}$$

$$\hat{\boldsymbol{\epsilon}}^{(r)}(\mathrm{p}) = \hat{\boldsymbol{\kappa}}^{(r)^{-1}} + \epsilon_0\mathbf{I}, \tag{25}$$

$$\hat{\mathbf{h}}^{(r)}(\mathrm{p}) = \frac{1}{2}(\hat{\mathbb{S}}^{(r)}\mathbf{h}^{(r)}\boldsymbol{\kappa}^{(r)^{-1}} + \mathbb{S}^{(r)}\mathbf{h}^{(r)}\hat{\boldsymbol{\kappa}}^{(r)^{-1}}); \tag{26}$$

here, the superscript T denotes transposition between the first pair of indeces and the last index. Now, material parameters employed to model typical ferroelectric ceramics are usually such that $O(||\mathbb{C}^{(r)}||\times||\boldsymbol{\kappa}^{(r)}||)\gg O(||\mathbf{h}^{(r)}||^2)$, and therefore it is common practice to take

$$\hat{\mathbb{S}}^{(r)}\approx\mathbb{S}^{(r)}, \quad \hat{\boldsymbol{\kappa}}^{(r)}\approx\boldsymbol{\kappa}^{(r)}, \quad \hat{\boldsymbol{\epsilon}}^{(r)}\approx\boldsymbol{\epsilon}^{(r)} = \epsilon_0\mathbf{I} + \boldsymbol{\kappa}^{(r)^{-1}}, \quad \hat{\mathbf{h}}^{(r)}\approx\mathbb{S}^{(r)}\mathbf{h}^{(r)}\boldsymbol{\kappa}^{(r)^{-1}}, \tag{27}$$

which simplifies expression (26) considerably[1]. Indeed, the coupled constitutive relations then take the form

$$\boldsymbol{\varepsilon} = \mathbb{S}^{(r)}\boldsymbol{\sigma} + \hat{\boldsymbol{\varepsilon}}^{(r)} - \hat{\mathbf{h}}^{(r)}\mathbf{E} \quad \text{and} \quad \mathbf{D} = \boldsymbol{\epsilon}^{(r)}\mathbf{E} + \mathrm{p} - \hat{\mathbf{h}}^{(r)T}\boldsymbol{\sigma}, \tag{28}$$

while the evolution law for the irreversible polarization takes the form

$$\mathbf{E} - h_0^{(r)}\frac{\mathrm{p}}{1-\frac{|\mathrm{p}|}{p_s^{(r)}}} + \frac{3\varepsilon_s^{(r)}}{(p_s^{(r)})^2}\boldsymbol{\sigma}_d\mathrm{p} - \frac{1}{|\mathrm{p}|}\left[[\boldsymbol{\sigma}\cdot\hat{\mathbf{h}}^{(r)}(\mathrm{p})\mathbf{E}]\frac{\mathrm{p}}{|\mathrm{p}|} + \frac{|\mathrm{p}|}{p_s^{(r)}}\left(\mathbf{I}-\frac{\mathrm{p}}{|\mathrm{p}|}\otimes\frac{\mathrm{p}}{|\mathrm{p}|}\right)\frac{\mathbf{v}}{\kappa^{(r)}}\right]$$

[1] The material parameters provided in Table 1 below are such that $O(||\mathbb{C}^{(r)}||\times||\boldsymbol{\kappa}^{(r)}||)\sim 10\,O(||\mathbf{h}^{(r)}||^2)$. While the approach considered in this work can perfectly handle material properties of the form (23)–(26), the approximations (27) will be used to provide contact with previous works and to simplify the discussions of Section 5. It has been verified that these approximations do not produce qualitative changes in the predictions.

$$= \left[e_c^{(r)} + e_0^{(r)} \left| \frac{\dot{\mathrm{p}}}{\dot{p}_0^{(r)}} \right|^m \right] \frac{\dot{\mathrm{p}}}{|\dot{\mathrm{p}}|}, \tag{29}$$

where $\boldsymbol{\sigma}_d$ is the deviatoric part of the stress tensor and the vector $\mathbf{v}$ is given by

$$\mathbf{v} = 2\alpha_0 \left(\frac{\mathrm{p}}{|\mathrm{p}|} \cdot \mathbf{E} \right) (\mathbb{S}^{(r)}\boldsymbol{\sigma}) \frac{\mathrm{p}}{|\mathrm{p}|} + \alpha_0 \left(\frac{\mathrm{p}}{|\mathrm{p}|} \cdot (\mathbb{S}^{(r)}\boldsymbol{\sigma}) \frac{\mathrm{p}}{|\mathrm{p}|} \right) \mathbf{E} + \alpha_\perp \mathrm{tr}\,(\mathbb{S}^{(r)}\boldsymbol{\sigma})\mathbf{E} + 2\alpha_\parallel (\mathbb{S}^{(r)}\boldsymbol{\sigma})\mathbf{E}. \tag{30}$$

(*iii*) In practice, micromechanical studies on the piezoelectric response of ferroelectric composites assume that the irreversible polarization is uniform and fixed throughout the solid (e.g., Dunn and Taya, 1993; Spinelli and Lopez-Pamies, 2015). This uniform-polarization approximation amounts to taking

$$\mathfrak{e}^{(r)}(\boldsymbol{\varepsilon}, \mathbf{P}, \mathrm{p}) = \frac{1}{2}\boldsymbol{\varepsilon} \cdot \mathbb{C}^{(r)}\boldsymbol{\varepsilon} + \frac{1}{2}\mathbf{P} \cdot \boldsymbol{\kappa}^{(r)}\mathbf{P} + \boldsymbol{\varepsilon} \cdot \mathbf{h}^{(r)}\mathbf{P} \quad \text{and} \quad \varphi^{(r)}(\dot{\mathrm{p}}) = 0, \tag{31}$$

with

$$\mathbf{h}^{(r)} = \alpha_0^{(r)}\, \mathbf{n} \otimes \mathbf{n} \otimes \mathbf{n} + \alpha_\perp^{(r)}\, \mathbf{I} \otimes \mathbf{n} + \alpha_=^{(r)}\, \mathbf{n} \otimes_s \mathbf{I}, \tag{32}$$

where $\boldsymbol{\varepsilon}$ and $\mathbf{P}$ are referred to the fully polarized reference configuration of the solid, and the unit vector $\mathbf{n}$ denotes the direction of remanent polarization. The free energy density is then given by

$$\psi^{(r)}(\boldsymbol{\sigma}, \mathbf{E}, \mathrm{p}) = \frac{1}{2}\boldsymbol{\sigma} \cdot \hat{\mathbb{S}}^{(r)}\boldsymbol{\sigma} + \frac{1}{2}\mathbf{E} \cdot \hat{\boldsymbol{\epsilon}}^{(r)}\mathbf{E} - \boldsymbol{\sigma} \cdot \hat{\mathbf{h}}^{(r)}\mathbf{E}, \tag{33}$$

where the hatted tensors are given by expressions analogous to (23)–(26), and can be approximated by expressions (27).

3. The overall response

The focus of this work is on material systems where the characteristic size of the microstructural heterogeneities —particles or cavities— is much smaller than the characteristic size of the composite body. Thus, making use of concepts of homogenization theory, we can define an overall or *homogenized* response of the composite material as the relation between conjugate fields averaged over a 'representative volume element' (RVE) Ξ which contains a sufficient number of heterogeneities for the overall response to be effectively independent of the prevalent conditions on its boundary (Germain et al., 1983; Hill, 1963).

We now invoke the variational representation of Miehe and Rosato (2011) for the overall response of heterogeneous solids with hereditary behavior. In this representation, the field equations are discretized in time ($t_0 = 0, t_1, \ldots, t_n, t_{n+1}, \ldots, t_N = T$) following an implicit Euler scheme, and the constitutive relations (11) are expressed as

$$\mathbf{D}_{n+1} = \frac{\partial w}{\partial \mathbf{E}}(\mathbf{x}, \boldsymbol{\sigma}_{n+1}, \mathbf{E}_{n+1}; \mathrm{p}_n) \quad \text{and} \quad \boldsymbol{\varepsilon}_{n+1} = \frac{\partial w}{\partial \boldsymbol{\sigma}}(\mathbf{x}, \boldsymbol{\sigma}_{n+1}, \mathbf{E}_{n+1}; \mathrm{p}_n), \tag{34}$$

where w is an incremental potential defined by

$$w(\mathbf{x}, \boldsymbol{\sigma}, \mathbf{E}; \mathrm{p}_n) = \sum_{r=1}^{2} \chi^{(r)}(\mathbf{x}) w^{(r)}(\boldsymbol{\sigma}, \mathbf{E}; \mathrm{p}_n) \tag{35}$$

with

$$w^{(r)}(\boldsymbol{\sigma}, \mathbf{E}; \mathrm{p}_n) = \sup_{\mathrm{p}} \left[\psi^{(r)}(\boldsymbol{\sigma}, \mathbf{E}, \mathrm{p}) - \Delta t\, \varphi^{(r)}\left(\frac{\mathrm{p} - \mathrm{p}_n}{\Delta t} \right) \right]. \tag{36}$$

In this expression, $\Delta t = t_{n+1} - t_n$ is the time step. The maximizing p in (36) is the irreversible polarization at time t_{n+1} which solves the discretized evolution law $(11)_2$.

Given the potential structure of the discretized constitutive relations (34), the corresponding macroscopic quantities are related by

$$\overline{\mathbf{D}}_{n+1} = \frac{\partial \widetilde{w}}{\partial \overline{\mathbf{E}}}(\overline{\boldsymbol{\sigma}}_{n+1}, \overline{\mathbf{E}}_{n+1}; \mathrm{p}_n) \quad \text{and} \quad \overline{\boldsymbol{\varepsilon}}_{n+1} = \frac{\partial \widetilde{w}}{\partial \overline{\boldsymbol{\sigma}}}(\overline{\boldsymbol{\sigma}}_{n+1}, \overline{\mathbf{E}}_{n+1}; \mathrm{p}_n), \tag{37}$$

where

$$\widetilde{w}(\overline{\boldsymbol{\sigma}}, \overline{\mathbf{E}}; \mathrm{p}_n) = \min_{\mathbf{E} \in \mathcal{K}(\overline{\mathbf{E}})} \min_{\boldsymbol{\sigma} \in \mathcal{S}(\overline{\boldsymbol{\sigma}})} \langle w(\mathbf{x}, \boldsymbol{\sigma}, \mathbf{E}; \mathrm{p}_n) \rangle \tag{38}$$

is an *incremental effective potential*. In this expression, $\langle \cdot \rangle$ denotes volume average over Ξ, $\mathcal{K}(\overline{\mathbf{E}})$ denotes the set of compatible electric fields $\mathbf{E}$ with volume average $\langle \mathbf{E} \rangle = \overline{\mathbf{E}}$, and $\mathcal{S}(\overline{\boldsymbol{\sigma}})$ denotes the set of statically admissible fields $\boldsymbol{\sigma}$ with volume average $\langle \boldsymbol{\sigma} \rangle = \overline{\boldsymbol{\sigma}}$. In turn, the conjugate macroscopic quantities are such that $\overline{\mathbf{D}} = \langle \mathbf{D} \rangle$ and $\overline{\boldsymbol{\varepsilon}} = \langle \boldsymbol{\varepsilon} \rangle$. Expression (37) constitutes the overall instantaneous response of the solid, which is completely characterized by the effective potential $\widetilde{w}$. The complete overall response is obtained by solving the minimization problem (38) for given p_n at each time step and integrating (37) in time. Note that despite appearances, the effective potential does not correspond strictly to a two-phase composite but rather to a composite with an infinite number of phases —this was initially observed by Lahellec and Suquet (2007) in the context of viscoelasticity. This is because the field p_n is, in general, heterogeneous even within each constituent phase. A priori, this conflicts with one of the practical purposes of homogenization procedures, which is to generate a simple description of the overall response in terms of a reduced number of macroscopic variables. However, the special class of material systems considered in the next section are peculiar precisely in that the local fields, including p_n, exhibit discrete distributions and, consequently, the overall response depends on a finite number of macroscopic variables.

4. A sequentially laminated model for particulate composites

A sequential laminate is an iterative construction obtained by layering laminated materials (which in turn have been obtained from lower-order lamination procedures) with other laminated materials, or directly with the homogeneous phases that make up the composite. The *rank* of the laminate refers to the number of layering operations required to reach the final sequential laminate. Given our interest in two-phase composites comprised of a continuous matrix containing a random dispersion of inclusions, we make use of the sequence of Idiart (2008, 2014). In this sequence, a rank-1 laminate corresponds to a simple laminate with a given layering direction $\mathbf{n}_1$, with phases 1 and 2 in proportions $(1 - f_1)$ and f_1. A rank-2 laminate is constructed by layering the rank-1 laminate with the matrix material $r = 1$, along a layering direction $\mathbf{n}_2$, in proportions f_2 and $1 - f_2$, assuming that the length scale of the *embedded* laminate is much smaller than the length scale of the *embedding* laminate. A rank-M laminate is obtained by repeating this process M times, always laminating a rank-m laminate with matrix material $r = 1$, in proportions f_m and $(1 - f_m)$, respectively, along a layering direction $\mathbf{n}_m$. Making repeated use of the well-known solution for simple laminates and the iterated homogenization theorem, it can be shown —see Idiart (2008, 2014) for derivations in the contexts of viscoplasticity and rigid ferroelectricity— that the incremental effective potential of the rank-M laminate is given by

$$\widetilde{w}(\overline{\boldsymbol{\sigma}}, \overline{\mathbf{E}}; \mathrm{p}_n) = \min_{\substack{a_i \in \mathbb{R} \\ i=1,\ldots,M}} \min_{\substack{\boldsymbol{\omega}_i \in \mathcal{S}(\mathbf{n}_i) \\ i=1,\ldots,M}} \left\{ c^{(2)} w^{(2)}\left(\overline{\boldsymbol{\sigma}}^{(2)}, \overline{\mathbf{E}}^{(2)}; \mathrm{p}_n^{(2)} \right) + c^{(1)} \sum_{i=1}^{M} \alpha_i\, w^{(1)}\left(\overline{\boldsymbol{\sigma}}_i^{(1)}, \overline{\mathbf{E}}_i^{(1)}; \mathrm{p}_{n,i}^{(1)} \right) \right\}, \tag{39}$$

where $\mathcal{S}(\mathbf{n}) = \{\boldsymbol{\omega} \text{ such that } \boldsymbol{\omega}\mathbf{n} = \mathbf{0}\}$, and

$$c^{(2)} = 1 - c^{(1)} = \prod_{i=1}^{M} f_i \quad \text{and} \quad \alpha_i = \frac{(1-f_i)}{f_i} \frac{\prod_{j=i}^{M} f_j}{1 - \prod_{j=1}^{M} f_j} \tag{40}$$

are microstructural variables representing, respectively, the total volume fractions $c^{(r)} = \langle \chi^{(r)}(\mathbf{x}) \rangle$ of each material r —such that $c^{(1)} + c^{(2)} = 1$— and the fraction of matrix material added at the i^{th} lamination —such that $\alpha_i > 0$ and $\sum_{i=1}^{M} \alpha_i = 1$—. In turn, the electric field intensities and the stress tensors are given by

$$\begin{aligned}
\overline{\mathbf{E}}_i^{(1)} &= \overline{\mathbf{E}} + a_i \mathbf{n}_i - \sum_{j=i}^{M} (1-f_j)\, a_j \mathbf{n}_j, \\
\overline{\boldsymbol{\sigma}}_i^{(1)} &= \overline{\boldsymbol{\sigma}} + \boldsymbol{\omega}_i - \sum_{j=i}^{M} (1-f_j) \boldsymbol{\omega}_j, \quad i = 1, \ldots, M,
\end{aligned} \tag{41}$$

$$\overline{\mathbf{E}}^{(2)} = \overline{\mathbf{E}} - \sum_{j=1}^{M} (1-f_j)\, a_j \mathbf{n}_j, \quad \overline{\boldsymbol{\sigma}}^{(2)} = \overline{\boldsymbol{\sigma}} - \sum_{j=1}^{M} (1-f_j) \boldsymbol{\omega}_j. \tag{42}$$

A key observation in deriving expression (39) by iteration was that the variational representation (38) is valid for local responses of the form (34) with any convex incremental potential —not necessarily of the form (36)—, and therefore include the macroscopic response (37). Note that the potential $w^{(2)}$ is evaluated at a single value of the electric field and irreversible polarization, while the potential $w^{(1)}$ is evaluated at M different values. This means that the fields are uniform within the inclusion phase $r = 2$ and discretely non-uniform within the matrix phase $r = 1$.

The incremental effective potential (39) depends on the volume fractions $c^{(r)}$ of each phase and on higher-order microstructural correlations through the set of microstructural quantities $\{(f_i, \mathbf{n}_i), i = 1, \ldots, M\}$. Thus, in order to use these constructions as model composites, the quantities $(f_i, \mathbf{n}_i)$ must be expressed in terms of the multipoint correlations of the microgeometries. However, this is not feasible in general. One strategy consists then in identifying subclasses of sequentially laminated constructions for which the dependence of the overall potential on higher-order correlations can be made explicit (Idiart, 2008; Idiart and Ponte Castañeda, 2013). Another strategy consists in identifying subclasses for which the overall potential exhibits desirable characteristics such as a certain symmetry group (Danas et al., 2008; deBotton and Hariton, 2002). In any event, it proves convenient to relate the quantities $(f_i, \mathbf{n}_i)$ to the so-called H-measures of the microgeometry $\mu^{(rs)}(\mathbf{n})$ $(r, s = 1, 2)$. These measures are geometrical objects that depend on the two-point correlation functions $\langle \chi^{(r)}(\mathbf{x}) \chi^{(s)}(\mathbf{x} - \mathbf{y}) \rangle$ of the microstructure; they quantify in phase space the lack of compactness of weakly converging sequences of characteristic functions $[\chi^{(r)}(\mathbf{x}) - c^{(r)}]$ and provide a partial characterization of microstructural oscillations along different directions in physical space (Tartar, 1990). For statistically uniform microstructures they are given by (Smyshlyaev and Willis, 1998)

$$\mu^{(rs)}(\mathbf{n}) = -\frac{1}{8\pi^2} \int_{\mathbb{R}^3} \delta''(\mathbf{n} \cdot \mathbf{x}) (\langle \chi^{(r)}(\mathbf{y}) \chi^{(s)}(\mathbf{y} - \mathbf{x}) \rangle - c^{(r)} c^{(s)})\, \mathrm{d}\mathbf{x}, \tag{43}$$

and for the particular class of sequentially laminated microgeometries considered here they take the form

$$\begin{aligned}
&\mu^{(rs)}(\mathbf{n}) = c^{(r)} (\delta_{rs} - c^{(s)}) \sum_{i=1}^{M} \nu_i\, \delta(\mathbf{n} - \mathbf{n}_i), \\
&\text{with} \quad \nu_i = \frac{1}{c^{(1)}} \frac{1-f_i}{f_i} \prod_{j=1}^{i} f_j,
\end{aligned} \tag{44}$$

where $\delta(\cdot)$ denotes the vector-valued Dirac delta function, and the ν_i are positive quantities such that $\sum_{i=1}^{M} \nu_i = 1$. Relations $(44)_2$ can be inverted to express the f_i in terms of the ν_i. Upon replacing the f_i in (39)–(42) by the ν_i, we obtain an alternative expression for the incremental effective potential $\widetilde{w}$ that depends on the underlying microgeometry through the total volume fractions $c^{(r)}$ of each material r and the set $\{(\nu_i, \mathbf{n}_i)\}$. The reader is referred to Idiart (2014) for further details.

If the incremental potentials $w^{(r)}$ are convex, the computation of the effective potential (39) for given macroscopic variables $\overline{\boldsymbol{\sigma}}$, $\overline{\mathbf{E}}$ and irreversible polarizations $\mathrm{p}_n^{(r)}$ requires the solution of a convex optimization problem with respect to a_i and $\boldsymbol{\omega}_i$. The corresponding conjugate variables $\overline{\mathbf{D}}$ and $\overline{\boldsymbol{\varepsilon}}$ can be then computed by differentiation; in view of the minimization conditions, it can be easily shown that

$$\begin{aligned}
\overline{\mathbf{D}} = \frac{\partial \widetilde{w}}{\partial \overline{\mathbf{E}}}(\overline{\boldsymbol{\sigma}}, \overline{\mathbf{E}}; \mathrm{p}_n) &= c^{(2)} \frac{\partial w^{(2)}}{\partial \mathbf{E}} \left(\overline{\boldsymbol{\sigma}}^{(2)}, \overline{\mathbf{E}}^{(2)}; \mathrm{p}_n^{(2)}\right) \\
&+ c^{(1)} \sum_{i=1}^{M} \alpha_i \frac{\partial w^{(1)}}{\partial \mathbf{E}} \left(\overline{\boldsymbol{\sigma}}_i^{(1)}, \overline{\mathbf{E}}_i^{(1)}; \mathrm{p}_{n,i}^{(1)}\right)
\end{aligned} \tag{45}$$

$$\begin{aligned}
\overline{\boldsymbol{\varepsilon}} = \frac{\partial \widetilde{w}}{\partial \overline{\boldsymbol{\sigma}}}(\overline{\boldsymbol{\sigma}}, \overline{\mathbf{E}}; \mathrm{p}_n) &= c^{(2)} \frac{\partial w^{(2)}}{\partial \boldsymbol{\sigma}} \left(\overline{\boldsymbol{\sigma}}^{(2)}, \overline{\mathbf{E}}^{(2)}; \mathrm{p}_n^{(2)}\right) \\
&+ c^{(1)} \sum_{i=1}^{M} \alpha_i \frac{\partial w^{(1)}}{\partial \boldsymbol{\sigma}} \left(\overline{\boldsymbol{\sigma}}_i^{(1)}, \overline{\mathbf{E}}_i^{(1)}; \mathrm{p}_{n,i}^{(1)}\right),
\end{aligned} \tag{46}$$

where the local fields are evaluated at the optimal solution. In addition, statistics of the local fields can be computed from expressions (41)–(42). In particular, the first and second moments of the intraphase stress distribution within each phase are given by

$$\langle \boldsymbol{\sigma} \rangle^{(1)} = \sum_{i=1}^{M} \alpha_i \overline{\boldsymbol{\sigma}}_i^{(1)} \quad \text{and} \quad \langle \boldsymbol{\sigma} \rangle^{(2)} = \overline{\boldsymbol{\sigma}}^{(2)}, \tag{47}$$

$$\langle \boldsymbol{\sigma} \otimes \boldsymbol{\sigma} \rangle^{(1)} = \sum_{i=1}^{M} \alpha_i \overline{\boldsymbol{\sigma}}_i^{(1)} \otimes \overline{\boldsymbol{\sigma}}_i^{(1)} \quad \text{and} \quad \langle \boldsymbol{\sigma} \otimes \boldsymbol{\sigma} \rangle^{(2)} = \overline{\boldsymbol{\sigma}}^{(2)} \otimes \overline{\boldsymbol{\sigma}}^{(2)}. \tag{48}$$

That these material systems represent the essential features of two-phase composites with particulate microstructures is supported by comparisons with full-field simulations and approximate estimates reported in various works on purely energetic/dissipative composites (e.g., deBotton and Hariton, 2002; Idiart, 2008; Idiart et al., 2006; Danas et al., 2008). Furthermore, when both phases are rigid ideal dielectrics, the effective potential (39) agrees exactly with the Maxwell-Garnett approximation —also known as the Claussius–Mossotti approximation— for two-phase linear dielectrics with H-measure $(44)_1$. Finally, if the uniform-polarization approximation (31) is employed, the effective potential (39) reduces to that of Spinelli and Lopez-Pamies (2015).

5. Sample results for representative material systems

The model presented above is used in this section to explore the influence of a second phase on the electro-deformability of polycrystalline ferroceramics. By way of example, we consider the extreme cases of metallic particles and microcavities. In both cases, the ferroelectric matrix is characterized by potentials of the form (16)–(22). On the other hand, the metallic particles are characterized as elastic perfect conductors, and the microcavities are assumed to be vacuous. Table 1 shows the numerical values adopted for the various material parameters. The values for the ferroelectric matrix roughly reproduce the rate-dependent behavior of a polycrystalline lead zirconate titanate at low frequencies (Miehe and Rosato, 2011; Zhou et al., 2001); the values for the metallic particles correspond to platinum. The second phase is assumed to be randomly and isotropically dispersed. Thus, we adopt the lamination sequence $\{\nu_i, \mathbf{n}_i\}$ considered by Idiart (2014) —see also Danas et al. (2008)— with rank $M = 250$. It is found

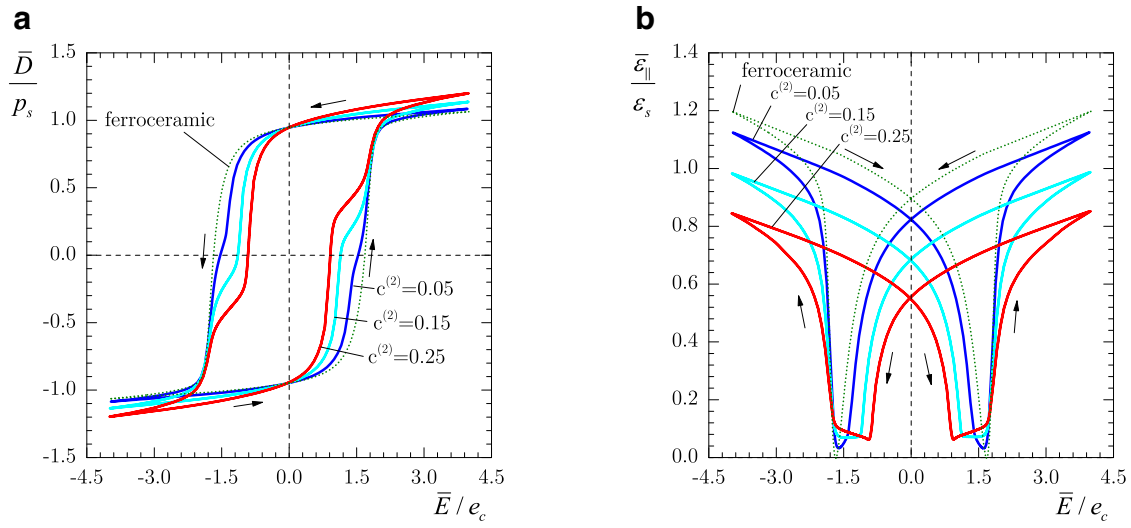

Fig. 1. Macroscopic response of a ferroceramic containing metallic particles at various volume fractions ($c^{(2)} = 0.05; 0.15; 0.25$): (a) electric displacement ($\overline{D}$) and (b) axial strain ($\overline{\varepsilon}$) as a function of the applied electric field intensity ($\overline{E}$). The quantities are normalized by the saturation polarization (p_s), saturation strain (ε_s), and coercive strength (e_c) of the ferroceramic matrix.

Table 1
Material parameters adopted. The values for the ferroelectric matrix roughly reproduce the rate-dependent behavior of a polycrystalline lead zirconate titanate at low frequencies; the values for the metallic particles correspond to platinum.

Symbol	Parameter	Units	Value
Ferroelectric matrix			
ϵ	Electric permittivity	C/(V·m)	$1800\epsilon_0$
p_s	Saturation polarization	C/m^2	0.25
h_0	Hysteresis slope	MV·m/C	0.1
m	Rate-sensitivity exponent	—	0.2
$\dot{p}_0$	Reference polarization rate	C/(m^2·s)	100
e_c	Coercive electric field	MV/m	0.35
e_0	Reference electric field	MV/m	0.35
μ	Lamé parameter	GPa	45
λ	Lamé parameter	GPa	70
ε_s	Saturation strain	—	10^{-3}
α_0	Axial piezoelectric expansion	MN/C	12.6
$\alpha_\perp$	Lateral piezoelectric expansion	MN/C	276
$\alpha_=$	Piezoelectric shearing	MN/C	−1460
Metallic inclusions			
ϵ	Electric permittivity	C/(V·m)	∞
μ	Lamé parameter	GPa	60
λ	Lamé parameter	GPa	225
Voided inclusions			
ϵ	Electric permittivity	C/(V·m)	ϵ_0
μ	Lamé parameter	GPa	0
λ	Lamé parameter	GPa	0

below that the resulting predictions percolate at $c^{(2)} = 1$; conclusions are therefore expected to be relevant to composites with a *polydisperse* second phase.

For each value of applied fields, the minimization in (39) with respect to the a_i and $\boldsymbol{\omega}_i$ is solved by means of a quasi-Newton optimization method for smooth, convex functions, while the irreversible polarizations in the potentials $w^{(r)}$ are computed by means of a direct search complex algorithm for nonsmooth, convex functions. In the case of metallic particles, the minimization with respect to the a_i is subject to the vectorial linear constraint $\overline{\mathbf{E}}^{(2)} = \mathbf{0}$ with $\overline{\mathbf{E}}^{(2)}$ given by $(42)_1$, while in the case of microcavities, the minimization with respect to $\boldsymbol{\omega}_i$ is subject to the tensorial linear constraint $\overline{\boldsymbol{\sigma}}^{(2)} = \mathbf{0}$ with $\overline{\boldsymbol{\sigma}}^{(2)}$ given by $(42)_2$.

5.1. Free-standing specimens

We begin by considering free-standing specimens subjected to a triangular electric signal with a peak amplitude of $4e_c$ and a frequency f_0 of 1Hz. The specimens are cycled from their initially unpoled state until the macroscopic response reaches a steady cycle, and then left unloaded until they reach their fully relaxed, permanently poled state[2]. The time step employed in the calculations is $\Delta t = 5 \times 10^{-3}$ s.

In reporting piezoelectric properties, the following standard notation for transversely isotropic systems is employed: $d_{33} = \partial\varepsilon_{\parallel}/\partial E$, $d_{31} = d_{32} = \partial\varepsilon_{\perp}/\partial E$, $d_h = d_{33} + d_{31} + d_{32}$, $g_{33} = \partial\varepsilon_{\parallel}/\partial D$, $g_{31} = g_{32} = \partial\varepsilon_{\perp}/\partial D$, and $g_h = g_{33} + g_{31} + g_{32}$. The symbols $\varepsilon_{\parallel}$ and $\varepsilon_{\perp}$ in these expressions refer to the normal strains along the parallel and perpendicular directions to the applied fields.

5.1.1. Ferroceramic with metallic particles

Fig. 1 shows the stabilized response predicted for various volume fractions of metallic particles ($c^{(2)} = 0.05, 0.15, 0.25$). The response of the monolithic ferroceramic is also provided as a reference. Part (a) shows plots for the macroscopic electric displacement in the direction of the applied electric field as a function of the applied electric field intensity, normalized by the saturation polarization and coercive strength of the matrix, respectively. It is observed that the macroscopic coercive strength of the composite decreases with increasing volume fraction of particles, as expected from the electric field enhancement within the matrix produced by the presence of a metallic phase. The macroscopic remanent polarization, on the other hand, is found to be relatively insensitive to the addition of metallic particles. This is consistent with the experimental observations of Duan et al. (2000) on PZT composites with Pt particles. Furthermore, these predictions are qualitatively identical to those obtained by Idiart (2014) for rigid dielectrics. Thus, as anticipated in that work, the local electromechanical coupling does not seem to influence the macroscopic electric response of freestanding specimens.

In turn, part (b) shows plots for the axial strain in the direction of the applied electric field, normalized by the saturation strain, as a function of the applied electric field intensity. The amplitude of the deformation cycle represents the electro-deformability of

[2] The specimen takes some time to reach the final equilibrium state in view of the electric viscosity.

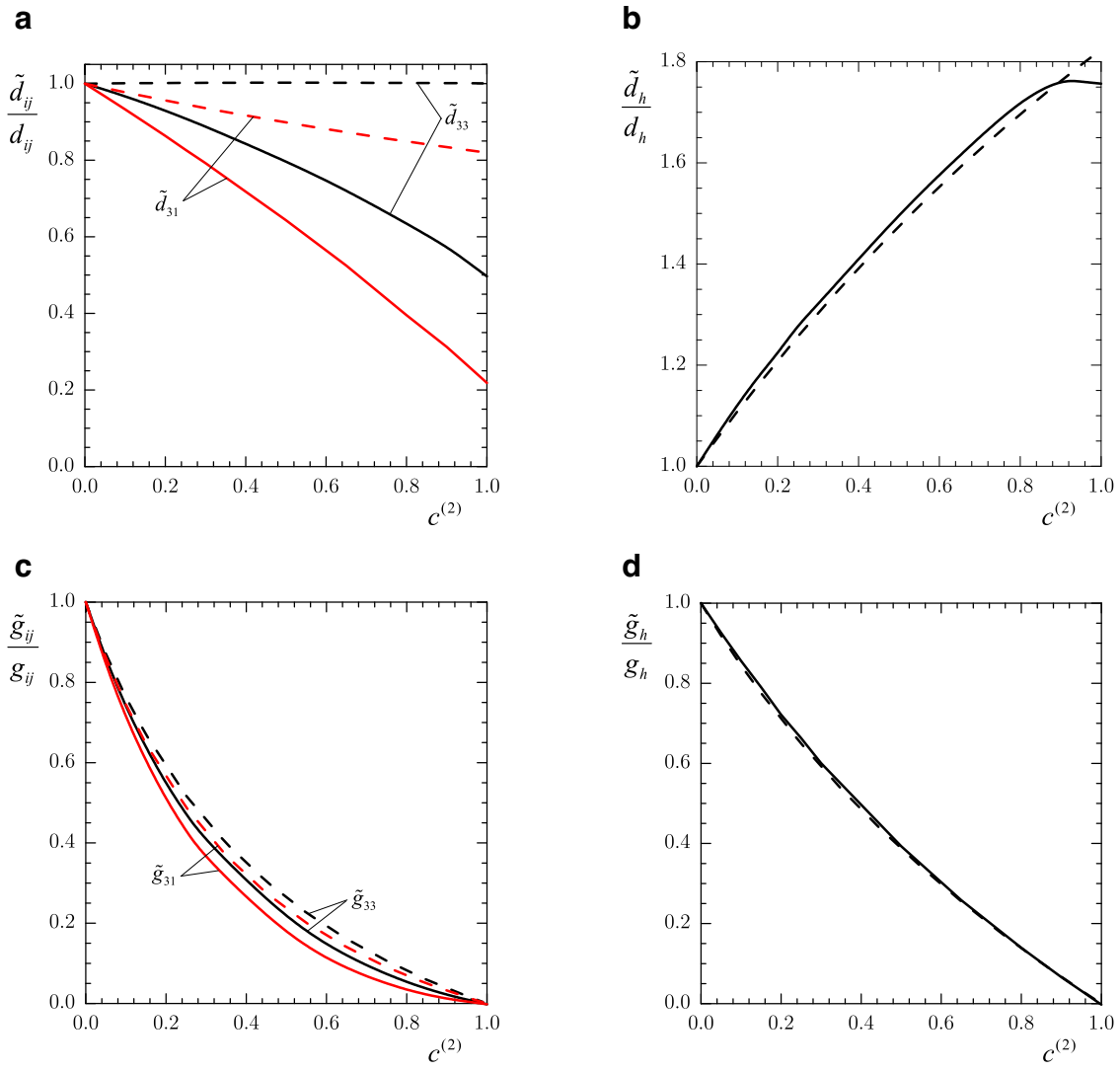

Fig. 2. Macroscopic piezoelectric coefficients of a permanently poled ferroceramic versus the volume fraction of metallic particles. Dotted lines correspond to the uniform-polarization approximation.

the composite. It is observed that the electro-deformability decreases with increasing volume fraction of particles. This electric-induced deformation is composed of a piezoelectric part and a ferroelectric switching part, as can be seen in expression (28). For the loading process considered here, however, the ferroelectric part is dominant. The decrease of the overall electro-deformability is a consequence of the fact that the ferroelectric deformation in the matrix phase, as given by expression (20), is proportional to the polarization squared and has the saturation strain as a limiting value. Thus, even though the addition of metallic particles enhances the electric field in the matrix phase, it does not produce larger electro-mechanical deformations in that phase, and at the same time it reduces the amount of bulk material exhibiting electro-mechanical coupling. Note that this mechanism will operate regardless of the elastic properties of the inclusion phase.

Fig. 2 shows corresponding predictions for macroscopic piezoelectric coefficients of the permanently poled specimen at the end of the loading program, as a function of particle volume fraction. These coefficients were calculated by differentiating numerically the macroscopic deformation with respect to the macroscopic electric field and electric displacement. The results are compared with the popular uniform-polarization approximation —dashed lines— using the same sequentially laminated microgeometries and material parameters. Addition of metallic particles is seen to be detrimental for all piezoelectric coefficients except the hydrostatic coefficient $\tilde{d}_h$. The predicted trends are consistent with those observed experimentally by Li et al. (2001) on PZT ceramics with Pt particles. The main observation in the context of this figure, however, is that the uniform-polarization approximation may not accurately capture the influence of metallic particles on the entire set of piezoelectric coefficients. Indeed, while the influence on the coefficients $\tilde{g}$ is well captured, the influence on the coefficients $\tilde{d}_{33}$ and $\tilde{d}_{31}$ is considerably underestimated. In fact, the uniform-polarization approximation misses out entirely the influence on the coefficient $\tilde{d}_{33}$ which, incidentally, is one of the most relevant coefficients for certain applications. Moreover, we have verified that re-scaling the piezoelectric coupling tensor for the matrix phase produces the same normalized results. The above inaccuracies can then be attributed to the neglect in the approximation of intraphase fluctuations of the permanent polarization within the matrix.

As a result of such fluctuations, residual stresses remain within the permanently poled composite. Predictions for the second moments of the intraphase residual stress distributions are given in Fig. 3a. The various curves correspond to the second moments of the norm $||\boldsymbol{\sigma}||$, the mean hydrostatic stress σ_m, and the von Mises equivalent stress σ_e, which can be computed by evaluating the following traces of the second-moment tensors (47)-(48): $\langle ||\boldsymbol{\sigma}||^2 \rangle^{(r)} = \mathbb{I} \cdot \langle \boldsymbol{\sigma} \otimes \boldsymbol{\sigma} \rangle^{(r)}$, $\langle \sigma_m^2 \rangle^{(r)} = (1/3)\ \mathbb{J} \cdot \langle \boldsymbol{\sigma} \otimes \boldsymbol{\sigma} \rangle^{(r)}$, $\langle \sigma_e^2 \rangle^{(r)} = (3/2)\ \mathbb{K} \cdot \langle \boldsymbol{\sigma} \otimes \boldsymbol{\sigma} \rangle^{(r)}$.

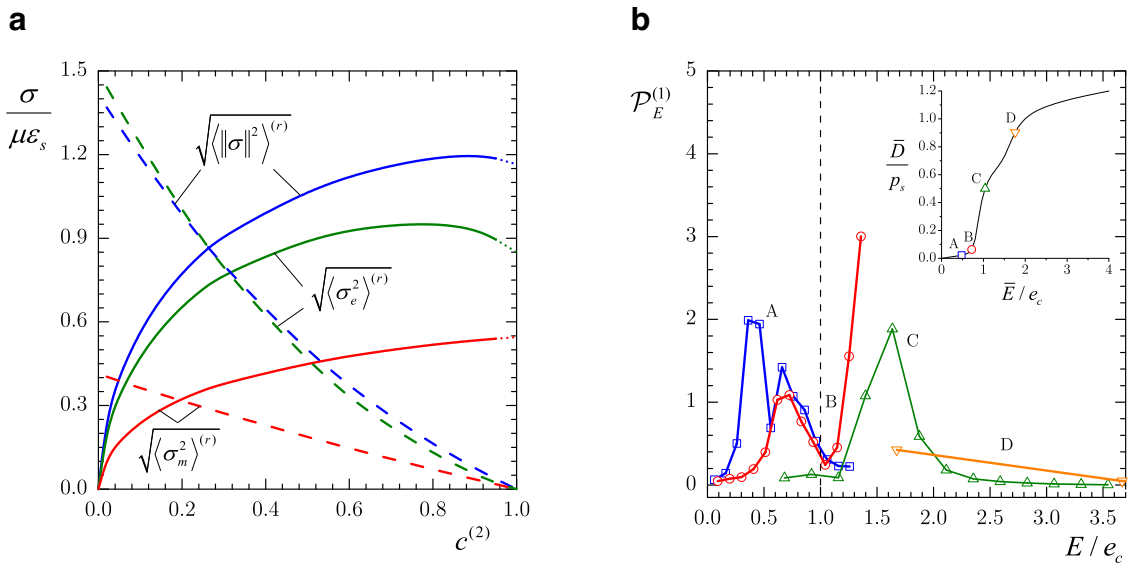

Fig. 3. Field statistics in a ferroceramic containing metallic particles: (a) second moments of the intraphase residual stress distributions versus volume fraction of particles, (b) probability density function for the distribution of electric field intensity within the matrix phase at various levels of applied field, for the choice $c^{(2)} = 0.25$.

Here, $\mathbb{J}$ and $\mathbb{K}$ are the standard fourth-order hydrostatic and shear projection tensors such that $\mathbb{I} = \mathbb{J} + \mathbb{K}$. Note that in view of these definitions the identity $\langle||\boldsymbol{\sigma}||^2\rangle^{(r)} = 3\langle\sigma_m^2\rangle^{(r)} + (2/3)\langle\sigma_e^2\rangle^{(r)}$ holds. Plots correspond to the square root of these quantities normalized by $\mu\varepsilon_s$. It can be seen that at low to moderate volume fractions of particles residual stresses are, on average, much larger in the inclusion than in the matrix phase, while the opposite holds at large volume fractions. Given the magnitude of $\mu\varepsilon_s$ for the material parameters of Table 1, these stress levels would be well below the mechanical strength of the metallic particles and the matrix-particle interface, but could be in the order of the mechanical strength of the ferroceramic matrix under tension. In this connection, it is noted that hydrostatic stresses within the matrix phase are found to be mostly of positive sign. In any event, uniform-polarization approaches neglect these residual stresses entirely and are therefore unable to inform any failure criteria.

We conclude this discussion by noting that, unlike the monolithic ferroceramic, the electric response of the composite shown in Fig. 1a exhibits a two-stage saturation which becomes more pronounced with increasing volume fraction of particles. This feature was already observed —but not explained— by Idiart (2014) in the context of rigid composites. Interestingly, it is also found in recent phase-field simulations of periodic composites (Keip et al., 2015). The feature can be ascribed to the bimodal character of the electric field intensity within the matrix phase. Fig. 3b shows the probability density function $\mathcal{P}_E^{(1)}(E)$ of the electric field intensity $E(\mathbf{x}) = |\mathbf{E}(\mathbf{x})|$ within the matrix phase[3], at four values of the applied electric field along the loading ramp from the initial unpoled state —see inset— for the choice $c^{(2)} = 0.25$. The probability densities were computed from the set of minimizing electric fields in (39) making use of the formulae of Idiart et al. (2006) —in order to have a sufficiently large set of local field values, these functions were obtained with sequential laminates of rank 3000. The bimodal character of the distribution and its evolution with applied loading is clearly observed. Thus, at state A, the two peaks sit at field intensities below the coercive strength so that the matrix is mostly unpoled and the macroscopic response is linear. At state B, the leading peak is sitting above the coercive strength level so that a large portion of the matrix is now undergoing switching and the macroscopic response suddenly increases in slope. At state C, the leading peak sits at the field intensity for which the matrix begins to saturate ($\sim 1.5e_c$) while the trailing peak still sits below the coercive strength; the macroscopic response exhibits a first saturation at this stage. But as the trailing peak crosses the coercive strength more matrix material undergoes switching and, consequently, the macroscopic response increases in slope once again. Finally, at state D, the entire electric field distribution lies well above the coercive strength so that the macroscopic response exhibits a second and final saturation. This bimodal distribution is also responsible for the distortion of the butterfly wells with increasing volume fraction of particles observed in Figure 1b. Bimodal electric field densities are also found in rigid ideal dielectrics with Hashin microgeometries, where the peaks can be associated with van Hove-type singularities of the electric field distribution within the matrix phase (Cule and Torquato, 1998). These microgeometries correspond to polydisperse particle distributions just like the sequentially laminated microgeometries considered here. By contrast, the electric field density function in rigid ideal dielectrics with monodisperse particle distributions is found to be unimodal (Cheng and Torquato, 1997), so that a two-stage saturation in the macroscopic response is not expected in this case. This is probably the reason why the experimental results of Duan et al. (2000) on PZT composites do not show such feature. In any event, knowledge on the character of the probability densities of the fields may prove useful not only in understanding the observed response but also in deriving simplified mean-field approximations following ideas of Pellegrini (2001).

5.1.2. *Ferroceramic with microcavities*

Fig. 4 shows predictions for various porosity levels ($c^{(2)} = 0.05, 0.15, 0.25$). Once again, the response of the monolithic ferroceramic is also provided as a reference. Part (a) shows normalized plots for the macroscopic electric displacement in the direction of the applied electric field as a function of the applied electric field intensity. It is observed that the macroscopic coercive strength is relatively insensitive to porosity, while the macroscopic remanent polarization decreases with increasing porosity. This is the exact opposite to the influence of the metallic particles observed in the previous section, and it is consistent with the experimental observations of Zeng et al. (2007) and Nie et al. (2010) on porous PZT ceramics.

[3] This function is such that $\mathcal{P}_E^{(1)}(E)\,\mathrm{d}\,E$ is the volume fraction of phase $r = 1$ where the variable E takes values in the range E and $E + \mathrm{d}\,E$.

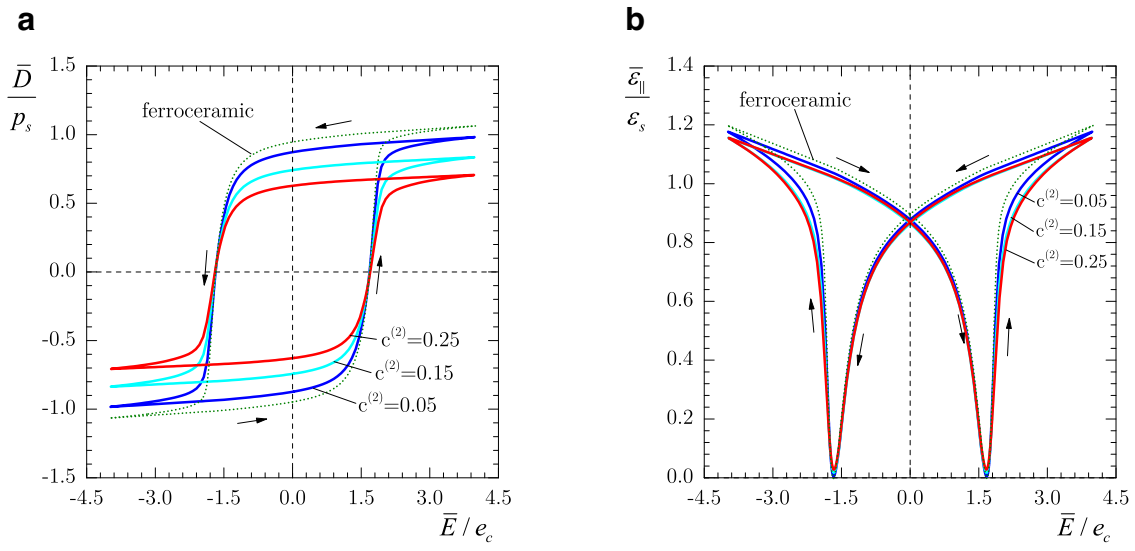

Fig. 4. Macroscopic response of a ferroceramic containing microcavities at various volume fractions ($c^{(2)} = 0.05; 0.15; 0.25$): (a) electric displacement ($\overline{D}$) and (b) axial strain ($\overline{\varepsilon}$) as a function of the applied electric field intensity ($\overline{E}$). The quantities are normalized by the saturation polarization (p_s), saturation strain (ε_s), and coercive strength (e_c) of the ferroceramic.

Furthermore, the predictions are qualitatively identical to those reported by Idiart (2014) for rigid dielectrics, which confirms that the local electromechanical coupling does not influence the macroscopic electric response of freestanding specimens.

In turn, part (b) shows normalized plots for the axial strain in the direction of the applied electric field as a function of the applied electric field intensity. In contrast to the case of metallic particles, the electro-deformability seems to be insensitive to porosity. However, the piezoelectric coefficients of the permanently poled specimens do vary strongly with porosity, as can be seen in Fig. 5. The presence of porosity is seen to be beneficial for all coefficients $\widetilde{g}$ and the hydrostatic coefficient $\widetilde{d}_h$. The trends are consistent with available experimental results for ferroceramics with closed porosity (Topolov and Bowen, 2009). It is emphasized, however, that the results do not apply to material systems with open porosity, where a much stronger influence of porosity on macroscopic properties is expected (Barolin et al., 2014). Finally, it is observed that, like in the case of metallic particles, the uniform-polarization approximation captures the right trends, being quite accurate for the coefficients $\widetilde{g}$, but underestimates somewhat the influence of porosity on the coefficients $\widetilde{d}_{33}$ and $\widetilde{d}_{31}$. Thus, the latter seems to be a common inaccuracy introduced by the approximation, at least in the context of particulate media.

Plots for the second moments of the residual stress distribution within the matrix phase are given in Fig. 6a; recall that the microcavities sustain no stress. Overall, the same trends as in the case of metallic particles are found, with the hydrostatic stress being mostly of the positive sign. However, a comparison with Fig. 3a shows that the residual stresses in the ferroelectric matrix are, on average, lower in the presence of microcavities than in the presence of metallic particles. This is opposite to what occurs in composites subject to mechanical loads, where stiffer inclusion phases induce lower stress levels in the matrix phase —see, for instance, Idiart et al. (2006).

We conclude this discussion by noting that the macroscopic electric response of Fig. 4a does not exhibit the two-stage saturation and butterfly distortion observed in the case of metallic particles. Fig. 6b shows the probability density function of the electric field intensity within the matrix phase at four values of the applied electric field. A unimodal character is clearly observed. The absence of a two-stage saturation in this case is thus consistent with the mechanism identified in the previous section.

5.2. Compressed specimens

We now consider specimens under the simultaneous action of electric fields and mechanical stresses. Polycrystalline PZTs can withstand compressive stresses well above 50 MPa (Munz et al., 1998). Thus, by way of example, we subject unpoled specimens to a uniaxial compressive stress of 50 MPa followed by a triangular electric signal with peak amplitude $4e_c$ and frequency of 1 Hz along the direction of the applied stress. The resulting predictions for material systems with metallic particles and microcavities at a volume fraction of $c^{(2)} = 0.25$ are reported in Fig. 7.

Parts (a) and (b) show the macroscopic axial strain as a function of the applied electric field for both types of material systems. Dotted lines correspond to the monolithic ferroceramic while solid lines correspond to the two-phase ferroceramics. Moreover, two sets of continuous lines are shown: blue lines correspond to a low-cycle response while red lines correspond to a high-cycle stabilized response. The main observation in the context of these figures is that, in contrast to the previous findings for free-standing specimens, the high-cycle stabilized response differs considerably from the low-cycle response, especially in the porous specimen. These differences, however, are not expected to be physically meaningful but rather a spurious result of the ill-defined energy density characterizing the ferroceramic matrix. As already noted in Section 2, the energy density (16) is not convex as required by the framework of generalized standard materials and, consequently, uniqueness of solutions to the incremental problem is not guaranteed.

It is precisely a non-uniqueness in the irreversible polarization evolution that results in the above odd behavior. Plots for the average irreversible polarization $\overline{\mathrm{p}}^{(1)}$ over the ferroceramic matrix are shown in parts (b) & (d). These plots show the maximum value over each electric cycle of the parallel and perpendicular projections of the vector $\overline{\mathrm{p}}^{(1)}$ to the axis of applied loads, as a function of cycle number. In view of the overall isotropy of the unpoled specimens, the vector $\overline{\mathrm{p}}^{(1)}$ should remain aligned with the axis of applied loads throughout the loading process; that is, the perpendicular projection should be zero. By contrast, the predictions show an exponential growth of the perpendicular projection up to a finite saturation value imposed by the local requirement that $|\mathrm{p}(\mathbf{x})| < p_s$. That this is a consequence of the non-convexity of the energy density (16) can be seen by evaluating the local evolution law (29) at a uniaxial stress σ and aligned electric

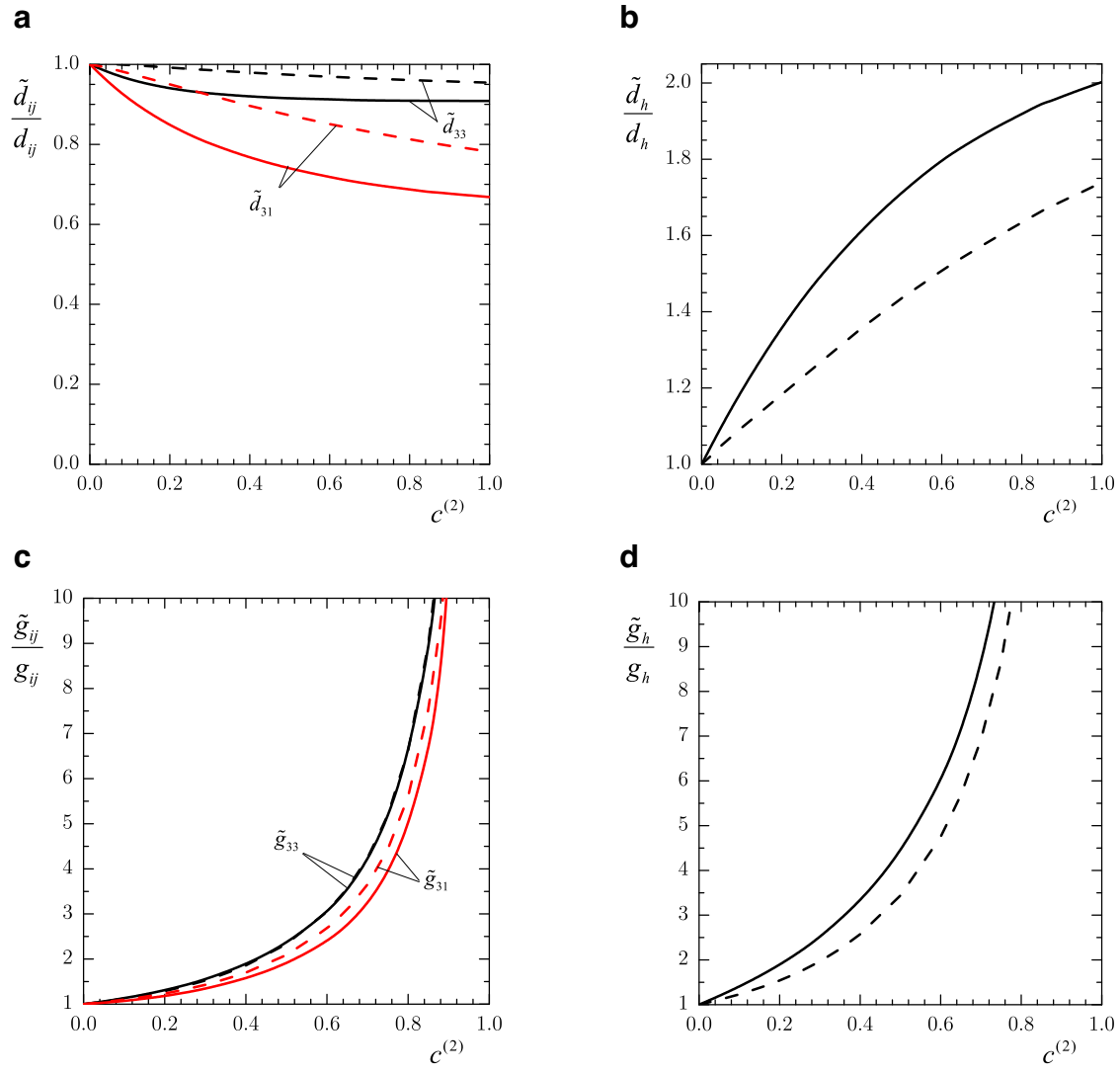

Fig. 5. Macroscopic piezoelectric coefficients of a permanently poled ferroceramic versus porosity. Dotted lines correspond to the uniform-polarization approximation.

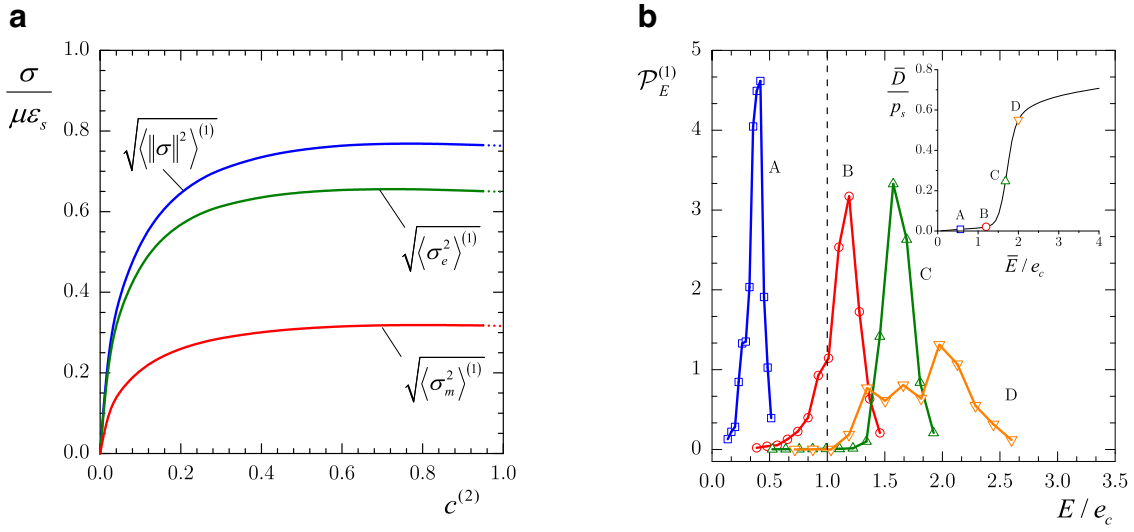

Fig. 6. Field statistics in a ferroceramic containing microcavities: (a) second moments of the intraphase residual stress distributions versus porosity, (b) probability density function for the distribution of electric field intensity within the matrix phase at various levels of applied field, for the choice $c^{(2)} = 0.25$.

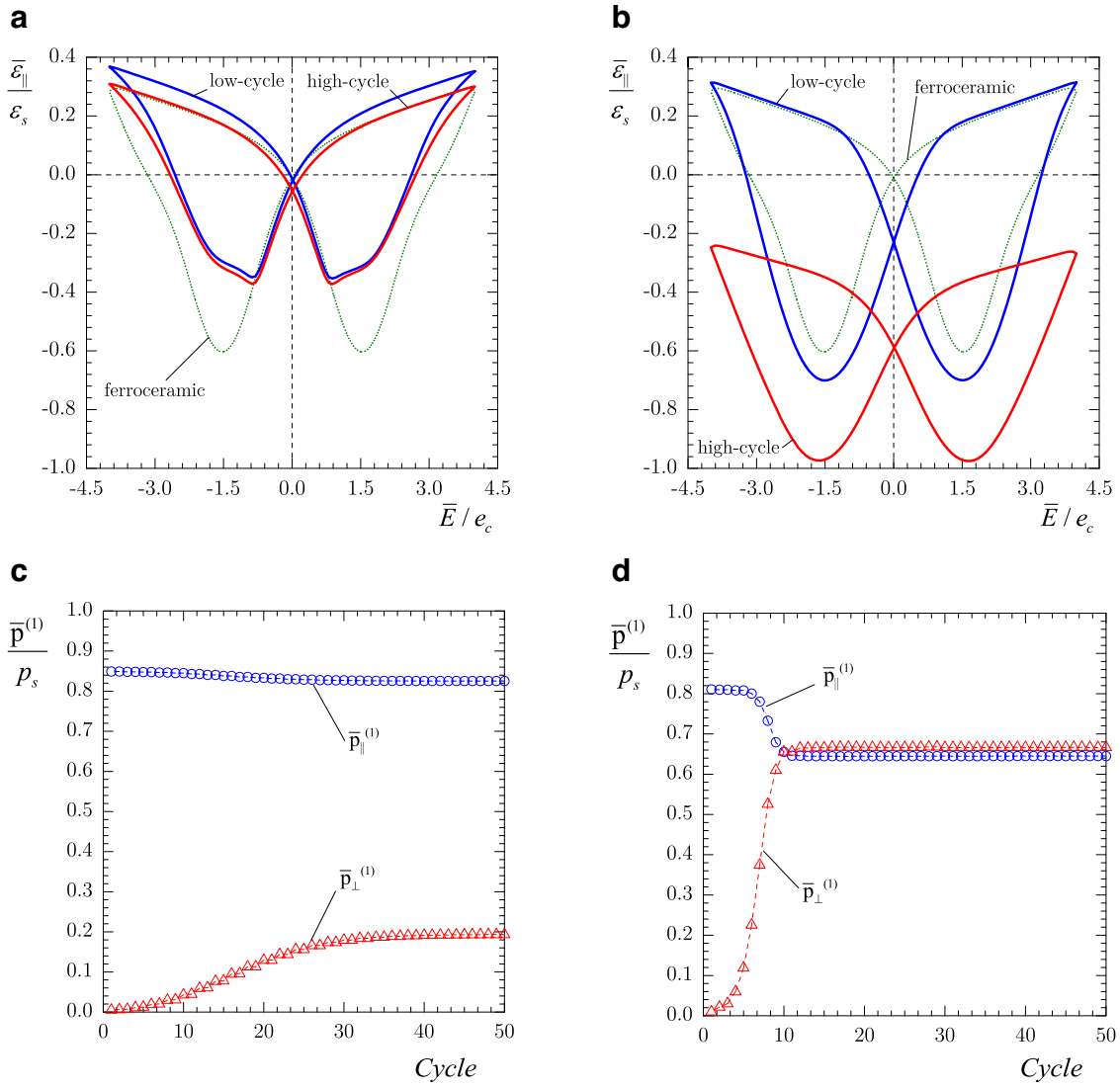

Fig. 7. Macroscopic axial strain ($\overline{\varepsilon}_{\parallel}$) and average irreversible polarization in the matrix phase ($\overline{\mathrm{p}}^{(1)}$) of compressed specimens with (a) & (c) metallic particles and (b) & (d) microcavities at a volume fraction of $c^{(2)} = 0.25$.

field E, and projecting it onto a perpendicular direction to the applied loads:

$$-\left[\frac{h_0}{1-\frac{|\mathrm{p}|}{p_s}}+\frac{\varepsilon_s}{p_s^2}\sigma\right]\mathrm{p}_{\perp}=\left[e_c+e_0\left|\frac{\dot{\mathrm{p}}}{\dot{p}_0}\right|^m\right]\frac{\dot{\mathrm{p}}_{\perp}}{|\dot{\mathrm{p}}|},\quad \mathrm{p}_{\perp}(0)=0. \tag{49}$$

The effect of piezoelectric coupling in this evolution law is negligible and has been omitted for clarity. It is evident that the trivial solution $\mathrm{p}_{\perp}(t)=0$ to Eq. (49) is stable provided the bracketed factor multiplying $\mathrm{p}_{\perp}$ on the left-hand side is positive. While this is the case for any tensile stress level ($\sigma > 0$), it is not the case for sufficiently large compressive stresses ($\sigma < 0$). This is likely to be the reason why the predictions for the free-standing specimens are found to be stable. In any event, this is a serious deficiency of the monolithic ferroelectric model, which can be pinned down to the relation (20) between the irreversible strain and polarization. In fact, the term depending on σ enters the evolution law (49) by virtue of the deviatoric operation in (20). Even though some propounders of relation (20) claim it is not intended for high stress levels —e.g., McMeeking and Landis (2002)—, expression (49) suggests non-uniqueness issues may arise for compressive stresses of the order of $\sim h_0 p_s^2/\varepsilon_s$, which can be a few megapascals for typical ferroceramics. Thus, ferroelectric models based on relation (20) should be used with caution even within their presumable range of validity.

Acknowledgements

This work was funded by the Agencia Nacional de Promoción Científica y Tecnológica through grant PICT-2011-0167 (M.I.I.) and by CONICET through a doctoral fellowship (C.J.B.). Additional support from the Universidad Nacional de La Plata through grant I-2013-179 is also gratefully acknowledged.

References

Barolin, S.A., De La Rubia, M.A., Terny, S., Rubio-Marcos, F., De Sanctis, O., Alonso, R.E., Fernández Lozano, J.F., De Frutos, J., 2014. Respuesta Ferro-Piezoelélectrica de (K,Na,Li)(Nb,Ta,Sb)O_3 Poroso. Blt. Soc. Esp. Cer. Vid. 53, 48–52.

Bassiouny, E., Ghaleb, A.F., Maugin, G.A., 1988. Thermodynamical formulation for coupled electromechanical hysteresis effects I. Basic equations.. Int. J. Eng. Sci. 26, 1279–1295.

Cheng, H., Torquato, S., 1997. Electric-field fluctuations in random dielectric composites. Phys. Rev. B 56, 8060–8068.

Cule, D., Torquato, S., 1998. Electric-field distribution in composite media. Phys. Rev. B 58 (R11), 829–832.

Danas, K., Idiart, M.I., Ponte Castañeda, P., 2008. A homogenization-based constitutive model for isotropic viscoplastic porous media. Int. J. Solids Struct. 45, 3392–3409.

deBotton, G., Hariton, I., 2002. High-rank nonlinear sequentially laminated composites and their possible tendency towards isotropic behavior. J. Mech. Phys. Solids 50, 2577–2595.
Duan, N., ten Elshof, J.E., Verweij, H., 2000. Enhancement of dielectric and ferroelectric properties by addition of Pt particles to a lead zirconate titanate matrix. App. Phys. Lett. 77, 3263–3565.
Dunn, M.L., Taya, M., 1993. Micromechanics predictions of the effective electroelastic moduli of piezoelectric composites. Int. J. Solids Struct 30, 161–175.
Germain, P., Nguyen, Q., Suquet, P., 1983. Continuum thermodynamics. J. Appl. Mech. 50, 1010–1020.
Hariton, I., deBotton, G., 2003. The nearly isotropic behaviour of high-rank nonlinear sequentially laminated composites. Proc. R. Soc. Lond. A 459, 157–174.
Hill, R., 1963. Elastic properties of reinforced solids: some theoretical principles. J. Mech. Phys. Solids 11, 357–372.
Idiart, M.I., 2008. Modeling the macroscopic behavior of two-phase nonlinear composites by infinite-rank laminates. J. Mech. Phys. Solids 56, 2599–2617.
Idiart, M.I., 2014. Modeling two–phase ferroelectric composites by sequential laminates. Model. Simul. Mater. Sci. Eng. 22, 025010.
Idiart, M.I., Moulinec, H., Ponte Castañeda, P., Suquet, P., 2006. Macroscopic behavior and field fluctuations in viscoplastic composites: second-order estimates versus full-field simulations. J. Mech. Phys. Solids 54, 1029–1063.
Idiart, M.I., Ponte Castañeda, P., 2013. Estimates for two-phase nonlinear conductors via iterated homogenization. Proc. R. Soc. A 469, 20120626.
Kamlah, M., 2001. Ferroelectric and ferroelastic piezoceramics – modelling of electromechanical hysteresis phenomena. Continuum Mech. Thermodyn. 13, 219–268.
Keip, M.-A., Schrade, D., Thai, H., Schröder, J., Svendsen, B., Müller, R., Gross, D., 2015. Coordinate-invariant phase field modeling of ferroelectrics, part II: application to composites and polycrystals. GAMM-Mitt. 38, 115–131.
Lahellec, N., Suquet, P., 2007. Effective behavior of linear viscoelastic composites: a time-integration approach. Int. J. Solids Struct. 44, 507–529.
Li, J.-F., Takagi, K., Terakubo, N., Watanabe, R., 2001. Electrical and mechanical properties of piezoelectric ceramic/metal composites in the $Pb(Zr,Ti)O_3$/Pt system. App. Phys. Lett. 79, 2441–2443.
McMeeking, R.M., Landis, C.M., 2002. A phenomenological multi-axial constitutive law for switching in polycrystalline ferroelectric ceramics. Int. J. Eng. Sci. 40, 1553–1577.
Miehe, C., Rosato, D., 2011. A rate-dependent incremental variational formulation of ferroelectricity. Int. J. Eng. Sci. 49, 466–496.
Munz, D., Fett, T., Müller, S., Thun, G., 1998. Deformation and strength behaviour of a soft PZT ceramic. In: SPIE 5th Conference on Smart Structures and Materials. San Diego (CA), U.S.A.
Nie, H.C., Dong, X.L., Feng, N.B., Chen, X.F., Wang, G.S., Gu, Y., He, H.L., Liu, Y.S., 2010. Quantitative dependence of the properties of $Pb_{0.99}(Zr_{0.95}Ti_{0.05})_{0.98}Nb_{0.02}O_3$ ferroelectric ceramics on porosity. Mater. Res. Bull. 45, 564–567.
Ning, X., Ping, P.Y., Zhuo, W., 2012. Large dielectric constant and Maxwell-Wagner effects in $BaTiO_3$/Cu composites. J. Am. Ceram. Soc. 95, 999–1003.
Pellegrini, Y.P., 2001. Self-consistent effective-medium approximation for strongly nonlinear media. Phys. Rev. B 64, 134211.
Piazza, D., Galassi, C., Barzegar, A., Damjanovic, D., 2010. Dielectric and piezoelectric properties of PZT ceramics with anisotropic porosity. J. Electroceram. 24, 170–176.
Smyshlyaev, V.P., Willis, J.R., 1998. A 'non-local' variational approach to the elastic energy minimization of martensitic polycrystals. Proc. R. Soc. Lond. A 454, 1573–1613.
Spinelli, S.A., Lopez-Pamies, O., 2015. A general closed-form solution for the overall response of piezoelectric composites with periodic and random particulate microstructures. Int. J. Solids Struct. 51, 2979–2989.
Tartar, L., 1990. H-measures, a new approach for studying homogenization, oscillation and concentration effects in partial differential equations. Proc. R. Soc. Edinb. A 115, 193–230.
Topolov, V.Y., Bowen, C.R., 2009. Electromechanical properties in composites based on ferroelectrics. Springer-Verlag, London, U.K..
Zeng, T., Dong, X.L., Mao, C.L., Zhou, Z.Y., Yang, H., 2007. Effects of pore shape and porosity on the properties of porous PZT 95/5 ceramics. J. Eur. Ceram. Soc. 27, 2025–2029.
Zhang, H., Yang, S., Zhang, B.-P., Li, J.-F., 2010. Electrical properties of Ni-particle-dispersed alkaline niobate composites sintered in a protective atmosphere. Mater. Chem. Phys. 122, 237–240.
Zhou, D., Kamlah, M., Munz, D., 2001. Rate dependence of soft PZT ceramics under electric field loading. In: Lynch, C. (Ed.), Proceedings of the SPIE 4333: Smart Structures and Materials, pp. 64–70.